16th World Conference on Earthquake, 16WCEE 2017

Santiago Chile, January 9th to 13th 2017

Paper N° 0411 (Abstract ID)

Registration Code: S-Y1461825545

DRIFT CAPACITY OF URM WALLS: ARE ANALYTICAL MODELS AN ALTERNATIVE TO EMPIRICAL APPROACHES?

B. Wilding[(1)], K. Beyer[(2)]

[(1)] *Phd-Student, École Polytechnique Fédérale de Lausanne, EESD, bastian.wilding@epfl.ch*
[(2)] *Assistant Professor, École Polytechnique Fédérale de Lausanne, EESD, katrin.beyer@epfl.ch*

Abstract

Code design of unreinforced masonry (URM) brick buildings is based on elastic analysis, which requires as input, among others, estimates of the in-plane drift capacity at the considered limit states. Current approaches assess the drift capacity of URM walls by means of empirical models with most codes relating the drift capacity to the failure mode and wall slenderness. Comparisons with experimental results show that such relationships result in large scatter and do not provide satisfactory predictions. The objective of this paper is to investigate whether analytical models could lead to more reliable estimates of the displacement capacity.

The drift capacity is investigated using a recently developed analytical model for the prediction of the ultimate drift capacity for both shear and flexure dominated URM walls. The approach is loosely based on plastic hinge models for reinforced concrete or steel structures. It takes the influence of toe crushing in URM walls explicitly into account as along with geometric and loading conditions. It is part of a more comprehensive model describing the whole force-displacement response of URM walls failing in shear or flexure.

This paper summarises the key features of this analytical drift capacity model and benchmarks its performance against a data set of 34 full scale wall tests. It shows that the analytical model yields significantly better estimates than empirical models in current codes. The paper concludes with an investigation of the sensitivity of the ultimate drift capacity to the wall geometry, static and kinematic boundary conditions by means of parametric studies.

Keywords: unreinforced masonry walls; ultimate drift capacity; shear dominated; flexure dominated

1 Introduction

Unreinforced masonry (URM) walls show in general either (i) a *flexure dominated* behaviour, characterised by a large displacement capacity and rocking of the wall with toe crushing as failure mode (Fig. 1a) or (ii) a behaviour that is *controlled by shear* with a rather limited displacement capacity. URM walls dominated by shear develop characteristic diagonal cracks (Fig. 1b). After reaching the peak load, the deformations tend to concentrate in a single crack and the force-displacement response of shear-controlled walls often shows a pronounced post-peak behaviour [1]. Characteristic horizontal load – horizontal displacement curves for walls developing these two failure modes are shown in Fig. 1c. The walls that determine the displacement capacity of a building are in general shear dominated walls, since they fail at a distinctively lower horizontal displacement than flexural dominated walls.

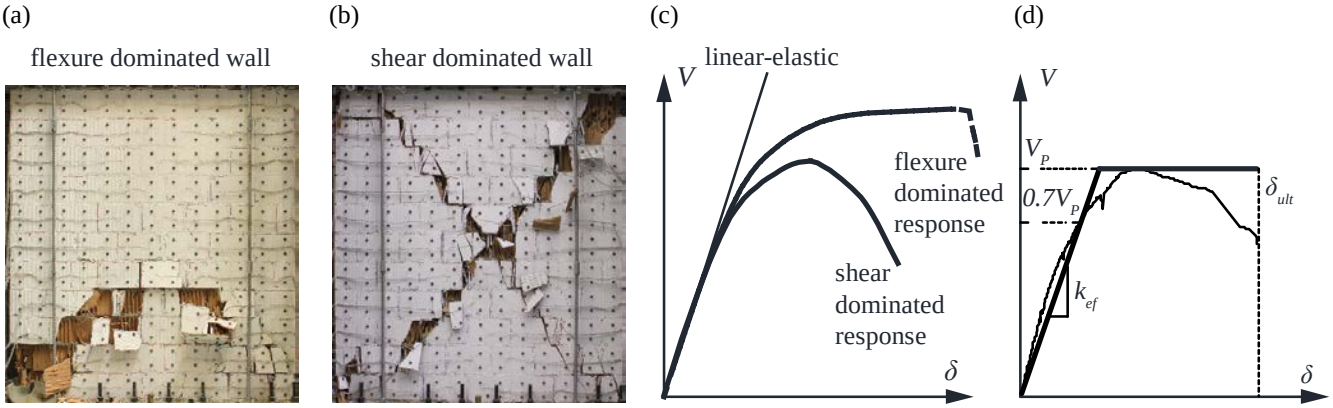

Fig. 1 – a Photo of flexure dominated wall at failure [1], b Photo of shear dominated wall at failure [1], c Shear load-drift curves qualitatively representing typical flexure and shear response of an in-plane loaded URM wall, d Monotonic shear load-drift response of a URM wall test in [1] as well as possible bi-linear approximation with indication of the effective stiffness (k_{ef}), the peak shear resistance (V_P) and the ultimate drift capacity (δ_{ult}).

Displacement-based design of URM walls loaded in-plane is conducted by approximating the strongly non-linear load-displacement histories by means of bi-linear curves (Fig. 1d). These bi-linear curves are defined by the effective stiffness, the peak strength and the ultimate drift capacity of the wall. The drift is defined as the horizontal displacement at the top of the wall divided by the wall height.

Many codes contain empirical drift capacity models for URM walls (e.g. Eurocode 8 [2], the Italian Code [3], the New Zealand Code [4], the American pre-standard FEMA 365 [5] and the Swiss Code [6]). Typically the drift capacity of walls is determined with empirical relations that depend on the failure mode (shear vs. flexure). Past studies have shown that such models lead to a large scatter of the results when compared to tests [1]. New formulations of empirical drift capacity models that account for other parameters than the failure mode can slightly improve the fit [7]–[9].

To improve the prediction of the drift capacity of URM walls, analytical formulations of the full load-displacement behaviour could be a remedy. So far, a number of formulations have been developed, either to be used as standalone beam element models to predict the response of single walls or to be used in equivalent frame analysis of buildings. Some of the most recently developed models are formulations presented in [10]–[15]. However, none of these models describes fully the load-displacement behaviour of shear critical URM walls including an estimate of the ultimate drift capacity, either since the formulation is only valid for flexural dominated walls or because only stiffness and strength but not the drift capacity are predicted.

2 Determination of the ultimate drift capacity

In this section, the novel analytical formulation in the CDC model to determine the ultimate drift capacity of URM walls is briefly introduced along with a short summary of the most commonly used empirical drift capacity models in codes.

2.1 New formulation

Both, flexure and shear controlled URM walls show a more or less extended crushed zone at the wall toe upon reaching ultimate failure (Fig. 1a, b). This leads to the concept of determining the ultimate drift capacity by means of a 'plastic zone' model, with very large curvatures in a confined zone at the wall toe. Yet, the approach of calculating these curvatures differs between shear and flexure dominated walls. Hence, it is necessary to explicitly predict the type of failure mode. It is assumed that the failure mode is controlled by the pre-peak behaviour. To predict the latter, the following assumptions are made: (i) masonry has zero tensile strength and hence, the parts of wall cross sections that would experience tension develop flexural cracking and decompression (as already applied in [11], [14]); (ii) masonry behaves linear elastically in compression; (iii) the wall can be analysed as a 2D-problem, i.e., the influence of out-of-plane bending is not considered.

2.1.1 Distinguishing between shear and flexure dominated walls

To distinguish between shear and flexural failure, it is proposed to consider the ratio between the height over which flexural decompression of the bed joints occurs (h_d) and half the wall height ($H / 2$) (see Fig. 2b). The height h_d can be determined as given in Eq. (1) with H_0 being the shear span and L the wall length.

$$h_d = \max\left[H_0 - \frac{NL}{6V_{ref}}, 0\right] \quad 1)$$

The variable h_d is computed for a reference shear force $V_{ref} = c\ L\ T$ (c – cohesion, T – wall thickness).

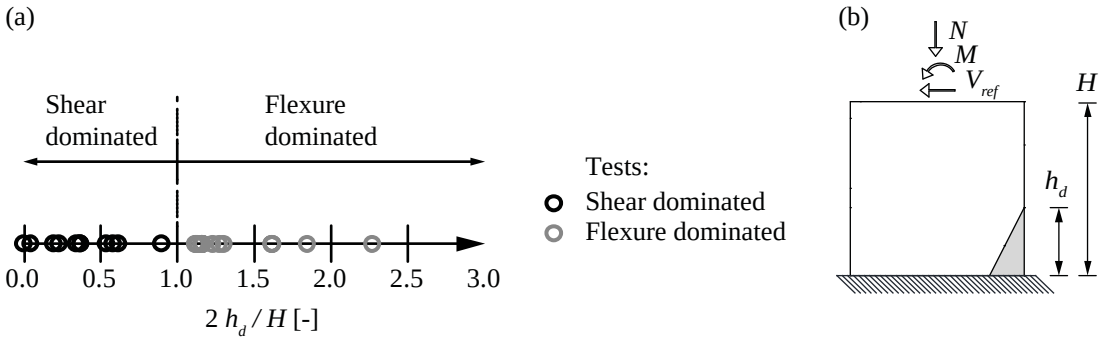

Fig. 2 – a The corresponding value of 2 h_d / H for tests that showed a shear dominated behaviour (black circles) and tests controlled by flexure (grey circles), b Sketch of decompressed height in wall at a reference shear force V_{ref} (grey hatch represents the decompressed area in the wall)

Substituting N with $\sigma_0\ L\ T$ and dividing Eq. (1) by $H / 2$ leads to (σ_0 – axial stress on wall)

$$\frac{2h_d}{H} = \frac{2H_0 - \frac{\sigma_0 L}{3c}}{H} \quad 2)$$

To verify whether the ratio $2h_d / H$ is indeed suitable for distinguishing between walls that fail in shear and walls that fail in flexure, it is applied to 34 tests for which the failure mechanisms are known (Table 2 in section 3). Fig. 2a shows that the ratio $2h_d / H$ allows to differentiate between these two types of behaviours. For a value of 2 $h_d / H < 1$, the walls tend to show a shear controlled behaviour in tests whereas for values larger than one, the walls exhibit a behaviour controlled by flexure.

2.1.2 Shear dominated walls

To obtain an estimate of the ultimate displacement capacity of a shear controlled URM wall, a plastic hinge approach accounting for its flexural displacements is adopted. URM walls with hollow clay bricks and normal cement mortar tend to fail due to crushing at the toe and along the diagonal crack (Fig. 3a, e.g. [1]).

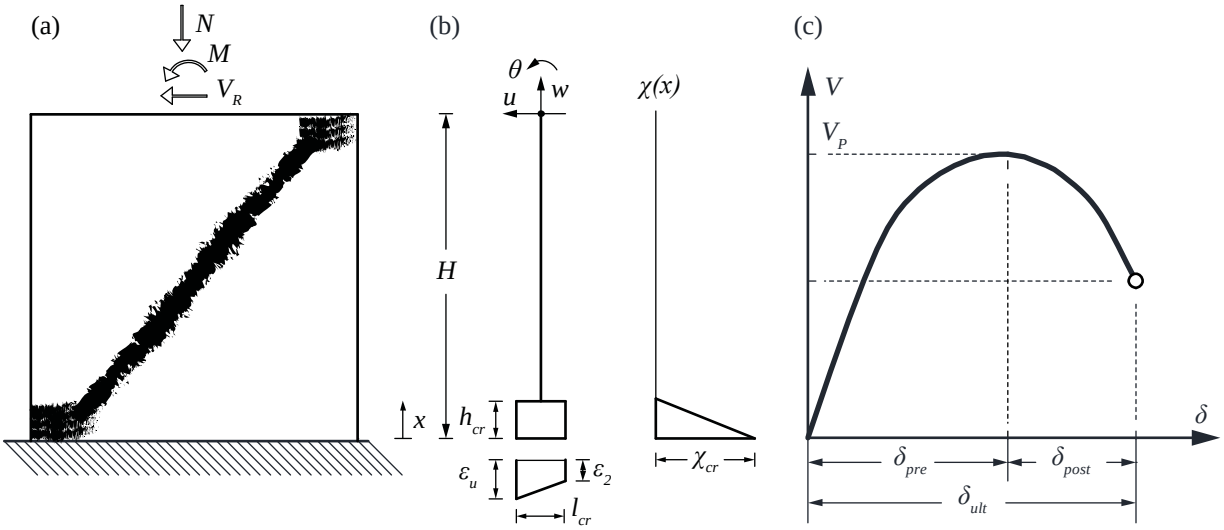

Fig. 3 – a Brick crushing in shear dominated wall at ultimate failure, b The considered equivalent system to determine the ultimate flexural displacements including assumed curvature profile, c Shear load-horizontal displacement curve, indicating point of ultimate failure

In the following, it is assumed that this crushed toe is responsible for the majority of displacements at ultimate failure. Hence, an equivalent system is introduced, which consists of a deformable zone at the wall toe defined by its crushed height (h_{cr}) and length (l_{cr}). It is assumed that the curvature distribution is linear over h_{cr} (Fig. 3b). At failure, the base curvature (χ_{cr}) is dependent on the maximum compressive strain (ε_u) of masonry as well as a strain (ε_2) taking into account the influence of the axial load. Furthermore, it is assumed that this curvature goes to zero approaching the height of the crushed zone (h_{cr}) as shown in the curvature profile provided in Fig. 3b. Curvatures above the crushed zone are assumed to be small compared to the one at the wall toe (χ_{cr}) and hence neglected. Moreover, shear displacements are assumed to be small compared to the flexural displacement components at ultimate failure and omitted as well.

The ultimate strain the material can sustain is estimated to roughly correspond to the ratio of the compressive strength of a brick and the elastic modulus of the material masonry with a maximum of 0.7 % as shown in Eq. (3).

$$\varepsilon_u \cong \min\left[\frac{f_{B,c}}{E}; 0.007\right] \quad 3)$$

Based on test observations, the length of the crushed zone (l_{cr}) is chosen to be the length of a brick (l_B). The strain ε_2 which is introduced at $y = l_{cr}$, as shown in Fig. 3b, is determined by means of vertical equilibrium.

$$\varepsilon_2 = \frac{2\sigma_0 L}{E l_{cr}} - \varepsilon_u \quad 4)$$

The height of the crushed zone (h_{cr}) is assumed to be dependent on the shear span (H_0), i.e. the higher the shear span ratio, the higher the crushed zone:

$$h_{cr} = h_B\left(\frac{1}{2} + \frac{H_0}{H}\right) \quad 5)$$

Based on the abovementioned assumptions, the rotation at the wall top, which is approximately equivalent to the ultimate horizontal drift (since the shear component is neglected), can be given as:

$$\delta_{ult} = \frac{1}{2}(\varepsilon_u - \varepsilon_2)\frac{h_{cr}}{l_{cr}}\left(1 - \frac{h_{cr}}{3H}\right) \quad 6)$$

The larger the axial stress, the smaller is the ultimate drift. This is in agreement with observations form experimental tests [1], [16], [17]. Eq. (6) also shows that the ultimate drift increases with increasing shear span, which has also been confirmed by experimental tests [8]. The mechanical model further indicates that the brick aspect ratio influences the ultimate drift. This is a point that could not yet be confirmed experimentally since it is difficult to vary the aspect ratio of bricks in tests systematically while keeping all other parameters the same.

2.1.3 Flexure dominated walls

Flexure controlled walls usually do not develop significant the load-displacement behaviour influencing diagonal cracks that are characteristic in shear dominated walls. They exhibit, however,—as shear walls do—a crushed zone at the wall toe upon reaching ultimate failure.

Due to the confinement effect of the foundation, the first and second row of bricks show different compressive strengths. This, however, leads to the possibility of various crushing mechanisms at the wall toe dependent on geometrical and loading conditions which are discussed in the following (see Fig. 4b1.1-1.3). The estimation of the ultimate drift for walls showing a flexure dominated behaviour will depend on the assumed respective mechanism.

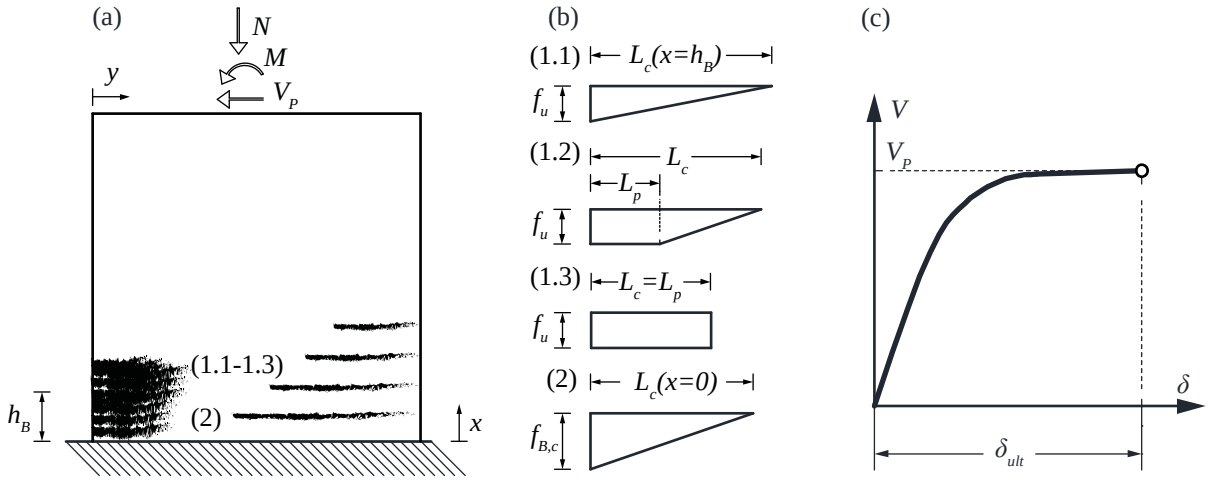

Fig. 4 – a Wall dominated by flexure at peak shear resistance with graphical representation of crushed wall toe and flexural cracks in bed joints, b1.1 Elastic normal stress distribution at the onset of crushing in the 2nd bed joint, b1.2 Assumed stress distribution for partly crushed zone in 2nd bed joint, b1.3 Corresponding assumed stress distribution for fully crushed compressed zone in 2nd bed joint, b2 Criterion for compression failure at wall toe, c Qualitative shear load – horizontal displacement curve indicating the point of peak shear resistance

Experimental evidence shows that in flexural dominated walls splitting cracks often start to form in the 2nd row of bricks [14]. These cracks, however, do not instantly lead to failure but the shear force can still be increased (e.g. [1]). The shear force at the onset of this crushing can be determined considering an elastic normal stress distribution in the second bed joint ($x = h_B$), reaching the masonry compressive strength (f_u) in the outermost fibre as shown in Fig. 4b1.1.

$$V(\sigma_{xx}(x = h_B, y = 0) = f_u) = \frac{NL}{2(H_0 - h_B)}\left(1 - \frac{4}{3}\frac{\sigma_0}{f_u}\right) \quad 7)$$

The tangent stiffness of the load-displacement curve at the point where crushing in the second row of bricks commences is usually already rather low, see Fig. 4c, which gives rise to the concept of considering the area where this preliminary crushing occurs as zone with a certain plastic deformation capacity (same concept as in [14]). As the shear force further increases, the length L_p of a plastic part of the normal stress distribution increases as well (see Fig. 4b1.2). It is assumed that failure is reached when the length L_p comprises the whole compressed length L_c and a fully plastic stress block has formed (Fig. 4b1.3). The corresponding shear force is:

$$V\left(L_c(x=h_B)=L_p(x=h_B)\right)=\frac{NL}{2(H_0-h_B)}\left(1-\frac{\sigma_0}{f_u}\right) \quad 8)$$

For walls with a rather high h_B / H ratio and / or a low level of axial loading (σ_0), the compressive stresses at the wall toe (x = 0, y = 0) can exceed the compression strength of the brick $f_{B,c}$ before the plastic zone in the second brick row has built up (Fig. 4b2). This is assumed to instantly cause failure of the wall. To consider this failure mode Eq. (9) is employed.

$$V\left(\sigma_{xx}(x=0,y=0)=f_{B,c}\right)=\frac{NL}{2H_0}\left(1-\frac{4}{3}\frac{\sigma_0}{f_{B,c}}\right) \quad 9)$$

All aforementioned conditions to determine the state of the normal stress distributions in the crushed zone in the second row of bricks at the onset of failure are summarised in Eq. (10).

$$\text{State} \rightarrow \begin{cases} \text{elastic} & \text{if } V\left(\sigma_{xx}(0,0)=f_{B,c}\right) < V(\sigma_{xx}(h_B,0)=f_u) \\ \text{partly plastic} & \text{if } V(\sigma_{xx}(h_B,0)=f_u) < V\left(\sigma_{xx}(0,0)=f_{B,c}\right) < V\left(L_c(h_B)=L_p(h_B)\right) \\ \text{fully plastic} & \text{if } V\left(\sigma_{xx}(0,0)=f_{B,c}\right) > V\left(L_c(h_B)=L_p(h_B)\right) \end{cases} \quad (10)$$

Fig. 5 shows the assumed curvature profiles along the wall height for the three different considered states. It is, once again, assumed that the curvatures above the crushed zones are negligible and that also shear displacements can be disregarded.

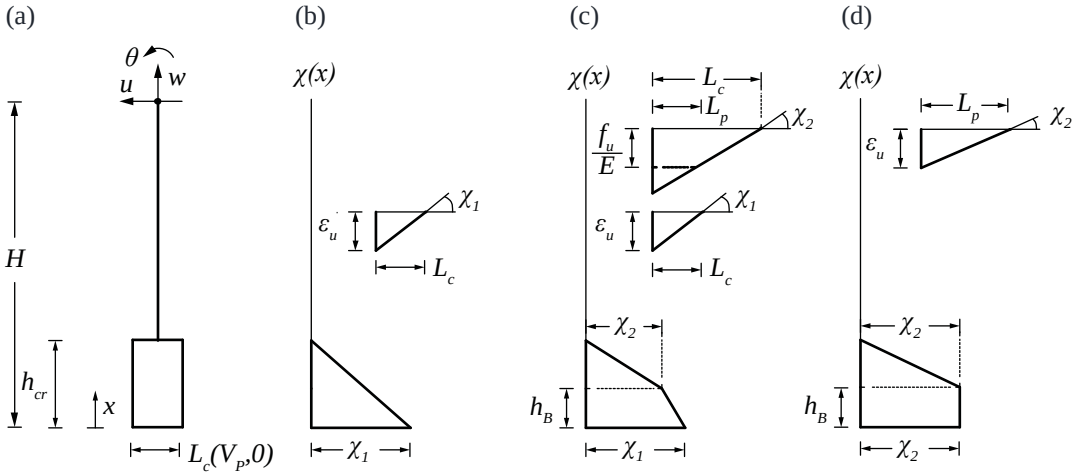

Fig. 5 – a Brick crushing at wall toe and flexural cracks in bed joints in flexure dominated wall at ultimate failure, b Assumed curvature profile of equivalent system if second row of bricks remains elastic, c Curvature profile if 2nd row of bricks is partly plastic, d Curvature profile if 2nd row of bricks is fully plastic stress block

The ultimate drift dependent on the state the 2nd row of bricks is in can be given as, see Fig. 5b-c:

$$\delta_{ult} \cong \begin{cases} \chi_1 \frac{h_{cr}}{2}\left(1-\frac{h_{cr}}{3H}\right) & h_B \text{ elastic, Fig. 5b} \\ \chi_1 \frac{h_B}{2}\left(1-\frac{h_{cr}}{H}+\frac{2h_B}{3H}\right)+\chi_2 \frac{h_{cr}}{2}\left(1-\frac{h_{cr}}{H}+\frac{2}{3H}\left(\frac{h_{cr}^2-h_B^2}{h_{cr}-h_B}\right)\right) & h_B \text{ par. pl., Fig. 5c} \\ \chi_2 \frac{h_B}{2}\left(1-\frac{h_{cr}}{H}+\frac{2h_B}{3H}\right)+\chi_2 \frac{h_{cr}}{2}\left(1-\frac{h_{cr}}{H}+\frac{2}{3H}\left(\frac{h_{cr}^2-h_B^2}{h_{cr}-h_B}\right)\right) & h_B \text{ ful. pl., Fig. 5d} \end{cases} \quad 11)$$

with the curvature at the base being:

$$\chi_1 = \frac{\varepsilon_u}{L_c(V_P,0)} \quad 12)$$

while the curvature in the 2nd bed joint can be estimated with:

$$\chi_2 = \begin{cases} min\left[\frac{f_u}{E\left(L_c(V_P,h_B)-L_p(V_P,h_B)\right)}, \frac{\varepsilon_u}{L_c(V_P,h_B)}\right] & h_B \text{ partly plastic} \\ \frac{\varepsilon_u}{L_c(V_P,h_B)} & h_B \text{ fully plastic} \end{cases} \quad 13)$$

The corresponding plastic compressed length in the 2nd bed joint is:

$$L_p(V_P,h_B) = \begin{cases} \frac{N-\sqrt{-3N^2+3f_uLTN-6f_uV_P(H_0-h_B)T}}{f_uT} & h_B \text{ partly plastic} \\ \frac{N}{f_uT} & h_B \text{ fully plastic} \end{cases} \quad 14)$$

with the total compressed length:

$$L_c(V_P,h_B) = \begin{cases} \frac{2N}{f_uT} - L_p(V_P,h_B) & h_B \text{ partly plastic} \\ L_p(V_P,h_B) & h_B \text{ fully plastic} \end{cases} \quad 15)$$

The compressed length at the wall base can be given as:

$$L_c(V_P,0) = 3\left(\frac{L}{2}-\frac{V_PH_0}{N}\right) \quad 16)$$

2.2 Drift capacity models in codes

2.2.1 Eurocode 8 (EC8)

EC8 – part 3 [2] gives an estimate for the drift at the *limit state of near collapse* ($\delta_{ult,EC}$), which is considered equivalent to the ultimate drift of the wall. The shear load carrying capacity of shear dominated walls is estimated in EC8 according to a modified Mohr-Coulomb criterion evaluating the compressed part of the base section using global values for coefficient of friction and cohesion. The peak shear resistance of walls controlled by flexure is determined using a stress block model assuming, again, that the critical section is the base joint. Whichever of those equations yield a smaller value is assumed to determine the behaviour of the wall (shear or flexure dominated) and hence implicitly the way of prediction of the ultimate drift capacity

$$\delta_{ult,EC8} = \begin{cases} \frac{4}{3}0.4\ [\%] & \text{for walls controlled by shear} \\ \frac{4}{3}0.8\ \frac{H_0}{L}[\%] & \text{for walls controlled by flexure} \end{cases} \quad (17)$$

2.2.2 German annex of EC8

The German annex reduces furthermore the drift capacities for walls failing in shear with a high axial load ratio.

$$\delta_{ult,GA,EC8} = \begin{cases} \frac{4}{3}0.4\ [\%] \text{ for} \frac{\sigma_0}{f_u} \leq 0.15 & \\ \frac{4}{3}0.3\ [\%] \text{ for} \frac{\sigma_0}{f_u} > 0.15 & \text{for walls controlled by shear} \\ \frac{4}{3}0.8\ \frac{H_0}{L}[\%] & \text{for walls controlled by flexure} \end{cases} \quad (18)$$

2.2.3 Italian Code NTC

The Italian code [3], however, simply sets two constant values dependent on the failure mode of the wall which is obtained nearly exactly corresponding to EC8.

$$\delta_{ult,NTC} = \begin{cases} 0.4\ [\%] & \text{for walls controlled by shear} \\ 0.8\ [\%] & \text{for walls controlled by flexure} \end{cases} \quad (19)$$

2.2.4 American pre-standard FEMA 365

The American pre-standard FEMA 365 [5] provides the Drift at Performance Level of Collapse Prevention (CP), which is supposed herein to be approximately equal to the ultimate drift capacity. It is distinguished between drift limits for URM walls failing in bed-joint sliding or rocking (which roughly corresponds to walls controlled by shear and walls controlled by flexure according to EC8). The failure mode is again determined by the minimum of corresponding equations determining the peak shear resistance of the wall.

$$\delta_{ult,FEMA\ 365} = \begin{cases} 0.4\ [\%] & \text{for bed-joint sliding} \\ 0.4\frac{H_0}{L}[\%] & \text{for rocking} \end{cases} \quad (20)$$

2.2.5 New Zealand Code

The New Zealand code [4] distinguishes between flanged and un-flanged walls (the only one doing so among the presented ones). Depending on the failure mode (designated shear failure mode and rocking or toe crushing failure mode in [4]) constant maximum permissible drift levels for un-flanged walls corresponding to the ones in the Italian code for the ultimate drift capacity are suggested. The failure mode is – in line with nearly all of the presented approaches – dependent on the minimum of equations describing the peak shear resistance of the wall.

$$\delta_{ult,NZSEE} = \begin{cases} 0.4\ [\%] \text{ for shear failure mode} \\ 0.8\ [\%] \text{ for rocking or toe crushing failure mode} \end{cases} \quad (21)$$

2.2.6 Swiss Code SIA D0237

According to the Swiss code SIA D0237 [6], the ultimate drift capacity of the wall is to be determined taking into account the boundary conditions a wall is subjected to without considering the predicted failure mode. The relation is given as follows:

$$\delta_{ult,SIA\ D0237} = \begin{cases} 0.4\left(1-\frac{\sigma_0}{f_u}\right)[\%] \text{ for fixed boundary condition: } \frac{H_0}{H}=0.5 \\ 0.8\left(1-\frac{\sigma_0}{f_u}\right)[\%] \text{ for cantilever boundary condition: } \frac{H_0}{H}=1 \end{cases} \quad (22)$$

3 Comparison with tests

The presented new formulation along with the abovementioned code provisions is compared to test campaigns of 34 full-scale quasi-static monotonic or cyclic URM wall tests to be found in literature (see Table 2) with regard to the prediction of the ultimate horizontal drift – δ_{ult}. A list of the tested walls *considered* for comparison is provided in Table 2. The walls were selected based on the following criteria: (i) wall height ≥ 1.5 m, (ii) wall length ≥ 1.0 m, (iii) constant shear span during test, (iv) constant axial load during test and (v) whether the envelope of the load-displacement history was available. Fig. 6 shows the performance of the CDC model as well as the code provisions presented in section 2.2 in predicting the ultimate drift capacity of the wall tests listed in Table 2. Since some of the tested walls (see Table 2) were subjected to other shear span ratios than 0.5 or 1, the upper term of Eq. (22) (drift capacity according to SIA D0237 [6]) is generally applied for a shear span ratio of $H_0 / H < 1$, while the lower one is taken for $H_0 / H \geq 1$ in the comparison.

Table 1 – Wall parameters used in the comparison of model/tests

Name	Ref.	Behaviour**	L [mm]	H [mm]	$H0/H$ [-]	h_B [mm]	l_B [mm]	σ_0 [MPa]	c [MPa]	f_u [MPa]	$f_{B,c}$ [MPa]	E [MPa]
PUP1		S			0.50			1.05				
PUP2		S			0.75			1.05				
PUP3	[1]	F	2010	2250	1.50	190	300	1.05	0.27	5.86	35.0	3550
PUP4		F			1.50			1.54				
PUP5		S			0.75			0.55				
BNW1		F	2567	1750		236	244	0.59				
BNW2		S	2572	1753		236	244	1.19				
BNW3	[17]	S	2584	1751	1.10	236	244	0.89	0.27#	5.86#	35.0#	5000#
BZW1		S	2482	1750		237	244	0.95				
BZW2		F	2484	1750		237	244	0.53				
BSW		S	2712	1820		188	288	2.07				
W1*		S			1.05			0.77				
W4*	[16]	F	3600	2000	2.00	190	300	0.78	0.27#	8.25	37.4	5000#
W6		S			1.05			0.77				
W7		S			1.05			2.39				
T1		S	2700		0.50			0.58				
T2		S	2700		0.50			0.29				
T3	[9]	S	2700	2600	0.50	190	290	1.16	0.26	5.80	26.3	3550#
T6		S	3600		0.50			0.58				
T7		F	2700		1.00			0.58				
BNL1		F	1028	1510		240	245	0.60		4.13	25.0#	3088
BNL2		F	1030	1510		240	245	1.19		4.13	25.0#	3088
BNL3		F	1033	1515		240	245	0.60		4.13	25.0#	3088
BNL4		F	1025	1514		240	245	1.19		4.13	25.0#	3088
BNL5		F	1027	1511		240	245	1.19		4.13	25.0#	3088
BNL6	[18]	F	1026	1508	1.06	240	245	0.60	0.27#	4.13	25.0#	3088
BGL1		F	989	1513		237	245	1.19		4.31	25.0#	3302
BGL2		F	987	1511		237	245	1.19		4.31	25.0#	3302
BPL1		F	985	1508		236	245	1.19		6.28	25.0#	4815
BPL2		F	985	1509		236	245	1.19		6.28	25.0#	4815
BPL3		F	986	1507		236	245	1.19		6.28	25.0#	4815

BZL1	F	988	1510		235	243	1.19	6.24	25.0#	5548
BZL2	F	987	1512		235	243	1.19	6.24	25.0#	5548
BZL3	F	986	1508		235	243	1.19	6.24	25.0#	5548

* walls were tested monotonically, all other walls cyclic, ** behaviour reported as hybrid or doubtful in reference assigned to F/S according to load-displacement response, where: F … flexure dominated behaviour, S … behaviour controlled by shear, # parameters assumed based on common values since either not provided in reference or as given values appeared not credible

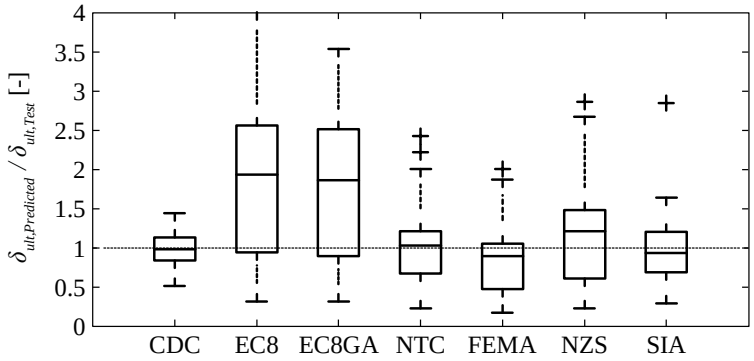

	CDC	EC8	EC8GA	NTC	FEMA	NZS	SIA
mean	0.97	1.81	1.73	1.06	0.89	1.20	0.99
st. dev.	0.21	0.99	1.00	0.53	0.47	0.69	0.47

Fig. 6 – Boxplot comparing performances of models in predicting ultimate drift capacity of tests

It is visible that the provisions according to EC8 strongly overestimate the drift capacities of the tested walls. The Italian code, the FEMA 365 as well as the NZ code show a large scatter as well but are not as overestimating. Of all the code provisions, the Swiss code yields the best result for the data set used for the comparison. Yet, the CDC model shows the best fit in predicting the ultimate drift capacities of all wall tests.

4 Parametric studies

In the following, parametric studies are conducted to investigate trends indicated by the CDC model concerning the ultimate drift capacity. Table 3 lists geometrical values and material parameters that are kept constant throughout the parametric analysis.

Table 2 – Values as used for all parametric studies

T [mm]	h_B [mm]	l_B [mm]	c [MPa]	f_u [MPa]	$f_{B,c}$ [MPa]	E [MPa]
200	190	300	0.27	5.86	35	3550

In Fig. 7, the shear span, axial load ratios as well as the wall size is varied while keeping the aspect ratio (ratio of H to L) the same. The ultimate drift capacity for walls with increasing size but constant H / L ratio is depicted in Fig. 7a. The shear span ratio is 0.5. It shows that the ultimate drift capacity decreases with increasing wall size, thus, agreeing with the size effect stipulated in [8]. The figure further shows that an increase in axial load leads to a reduced ultimate drift capacity. For Fig. 7b, the shear span ratio is set to 1.5. With increasing wall size, the ultimate drift decreases agreeing with the idea of a pronounced size effect for flexural walls (characterised by higher shear span ratios and lower levels of axial load). For a higher level of axial load, the size effect is not as strong anymore but still clearly discernible. Fig. 7b shows again the negative influence of the axial loading on the ultimate drift capacity. For comparison, Fig. 7 additionally provides the drift capacities according to EC8 along with those given in the Swiss code. Fig. 7a, b shows that such simple equations do not fully capture the aforementioned trends (size effect, influence of axial load ratio). The provisions of EC8 are generally un-conservative for the investigated wall parameters. The estimates of SIA D0237, however, are more

conservative and lie roughly in the range of the expected results as also reflected in the comparison part in section 3.

Fig. 7c represents the development of the ultimate drift capacity with changing axial load ratio keeping the wall size constant. For small shear span ratios ($H_0 / H = 0.5$ – usually corresponding to shear critical walls), the drift capacity decreases slightly with increasing axial load while for a high shear span ratio of 1.5 that is more characteristic of flexure controlled walls, the distribution of the drift capacities varies quite strongly. A low level of axial load leads to high ultimate drifts, in this case similar to the provisions given in EC8. However, these high drifts tend to decrease rapidly with increasing axial load ratio. The provisions according to the Swiss code somewhat take the dependency of the ultimate drift on the axial loading into account – for higher axial loads, the estimates of the CDC model and SIA nearly overlap while the non-linear relationship suggested by the CDC model for lower axial loads (and thus more flexure controlled walls) is just roughly approximated linearly by the provision according to SIA.

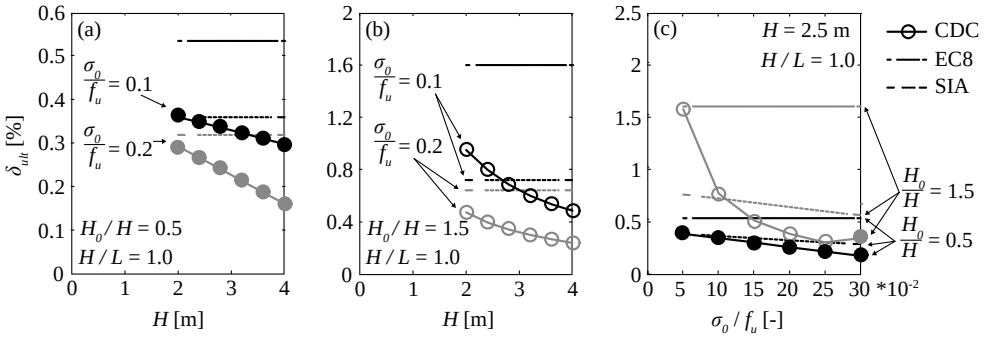

Fig. 7 – a and b Parametric study of ultimate drift capacity with changing wall size keeping aspect ratio and shear span constant, c Parametric study of ultimate drift capacity with changing axial load ratio keeping shear span and wall size – full markers indicate shear dominated, unfilled markers designate flexure controlled behaviour

Parametric studies investigating the influence of a changing wall aspect ratio on the ultimate drift capacity are presented in Fig. 8. The drifts increase with increasing H / L ratio. Moreover, as already mentioned above, the trend for higher drifts with lower axial load ratio is clearly visible. As for the provisions according to EC8, they are generally un-conservative for the parameters used in this study. They seem to fit best for small walls tested with a shear span ratio of one and low axial load ratios, i.e., for the wall configurations that have been tested very frequently and were therefore probably overrepresented in the data set used for determining the empirical drift capacity models [8]. Another detail that can be observed in Fig. 8a and b is that EC8 often assesses the type of wall behaviour (shear, flexure dominated) differently than the CDC model, i.e. EC8 classifies walls to be of the flexural dominated type while the CDC model still assigns them to the shear kind. The provisions of the Swiss code which are included in Fig. 8 as well just show constant drift levels depending on the shear span and axial loading. They do not follow the trends indicated by the CDC model but are more conservative than the provisions given in EC8.

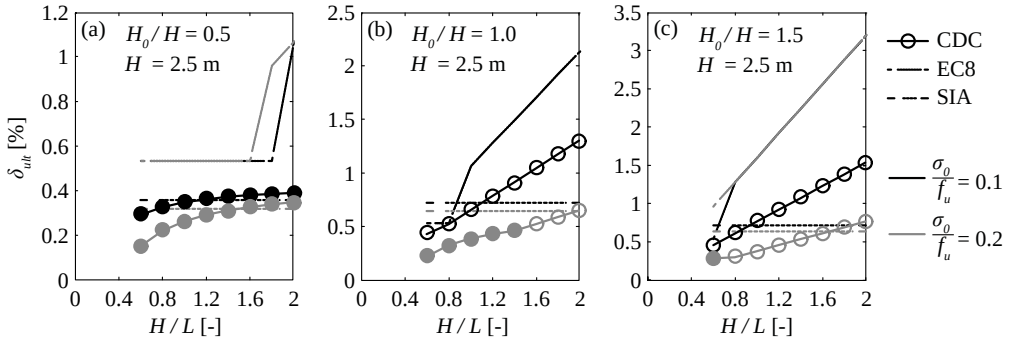

Fig. 8 – Development of ultimate drift with changing wall aspect ratio; a Shear span ratio of 0.5, b Shear span ratio of 1, c Shear span ratio of 1.5 – full markers indicate shear dominated, unfilled markers designate flexure controlled behaviour

5 Conclusion

A novel mechanics-based approach to determine the drift capacity of in-plane loaded URM walls which is part of a more comprehensive model describing the full monotonic load-displacement response—the CDC model—has been briefly introduced. The approach is based on an estimation of curvature profiles in the crushed zone at the wall toe at failure to determine the ultimate drift capacity. The comparison with 34 full-scale URM wall tests shows that the novel approach estimates the drift capacity of the walls more accurately than the empirical provisions used in current codes. A concluding parametric study shows that the predicted development of the drift capacity related to the change in different boundary conditions seems to agree well with behaviours observed in tests and stresses the influence of the axial loading, the shear span as well as the aspect ratio of the wall on its drift capacity which is not fully taken into account in code provisions.

6 References

[1] S. Petry and K. Beyer, “Cyclic Test Data of Six Unreinforced Masonry Walls with Different Boundary Conditions,” *Earthq. Spectra*, vol. 31, no. 4, pp. 2459–2484, Nov. 2015.

[2] CEN, “EN 1998-3: 2005 Eurocode 8: Design of structures for earthquake resistance - Part 3: Assessment and retrofitting of buildings,” Comité Européen de Normalisation, 2005.

[3] NTC, “Decreto Ministeriale 14/1/2008: Norme tecniche per le costruzioni,” Ministry of Infrastructures and Transportations, 2008.

[4] NZSEE, “Assessment and Improvement of Unreinforced Masonry Buildings for Earthquake Resistance, New Zealand Society of Earthquake Engineering, supplement to ‘Assessment and improvement of the structural performance of buildings in earthquakes,’” University of Auckland, 2011.

[5] ASCE, “FEMA 356 - Prestandard and Commentary for the Seismic Rehabilitation of Buildings,” American Society of Civil Engineers, Reston, Virginia, 2000.

[6] SIA, “SIA D0237: Evaluation de la sécurité parasismique des bâtiments en maçonnerie. Swiss Society of Engineers and Architects SIA,” Zürich, Switzerland, 2011.

[7] K. Lang, “Seismic vulnerability of existing buildings,” Phd-Thesis, ETH Zürich, 2002.

[8] S. Petry and K. Beyer, “Influence of boundary conditions and size effect on the drift capacity of URM walls,” *Eng. Struct.*, vol. 65, pp. 76–88, Apr. 2014.

[9] A. H. Salmanpour, N. Mojsilović, and J. Schwartz, “Displacement capacity of contemporary unreinforced masonry walls: An experimental study,” *Eng. Struct.*, vol. 89, pp. 1–16, Apr. 2015.

[10] S.-Y. Chen, F. L. Moon, and T. Yi, “A macroelement for the nonlinear analysis of in-plane unreinforced masonry piers,” *Eng. Struct.*, vol. 30, no. 8, pp. 2242–2252, Aug. 2008.

[11] A. Benedetti and E. Steli, "Analytical models for shear–displacement curves of unreinforced and FRP reinforced masonry panels," *Constr. Build. Mater.*, vol. 22, no. 3, pp. 175–185, Mar. 2008.

[12] I. Caliò, M. Marletta, and B. Pantò, "A new discrete element model for the evaluation of the seismic behaviour of unreinforced masonry buildings," *Eng. Struct.*, vol. 40, no. October 2015, pp. 327–338, Jul. 2012.

[13] E. Raka, E. Spacone, V. Sepe, and G. Camata, "Advanced frame element for seismic analysis of masonry structures: model formulation and validation," *Earthq. Eng. Struct. Dyn.*, vol. 44, no. 14, pp. 2489–2506, Nov. 2015.

[14] S. Petry and K. Beyer, "Force-displacement response of in-plane-loaded URM walls with a dominating flexural mode," *Earthq. Eng. Struct. Dyn.*, vol. 44, no. 14, pp. 2551–2573, Nov. 2015.

[15] A. Penna, S. Lagomarsino, and A. Galasco, "A nonlinear macroelement model for the seismic analysis of masonry buildings," *Earthq. Eng. Struct. Dyn.*, vol. 43, no. 2, pp. 159–179, Feb. 2014.

[16] H. Ganz and B. Thürlimann, "Versuche an Mauerwerksscheiben unter Normalkraft und Querkraft," Test Report, ETH Zürich, 1984.

[17] V. Bosiljkov, M. Tomazevic, and M. Lutman, "Optimization of shape of masonry units and technology of construction for earthquake resistant masonry buildings - Part Three," Lubljana, Slovenia, 2006.

[18] V. Bosiljkov, M. Tomazevic, and M. Lutman, "Optimization of shape of masonry units and technology of construction for earthquake resistant masonry buildings - Part One and Two," Lubljana, Slowenia, 2004.